International Research Journal of Multidisciplinary Scope (IRJMS), 2025; 6(1):867-878 IRJMS

Original Article | ISSN (O): 2582-631X DOI: 10.47857/irjms.2025.v06i01.02856

Effective CT Lung Image Denoising using Deep-Dense Inception Generative Adversarial Network

Narendra Lalchand Lokhande*, Tushar Hrishikesh Jaware

Department of Electronics and Telecommunication, R C Patel Institute of Technology, Shirpur, Maharashtra, India. *Corresponding Author's Email: narenlokhande@gmail.com

Abstract

Computed tomography (CT) is used to visualize body structures and diagnose anomalies, making it an important tool in medical diagnosis and therapy planning. However, imaging techniques such as CT, MRI, ultrasound (US), and PET are frequently hampered by numerous types of noise, including Gaussian, speckle, Poisson variability, and salt-and-pepper disturbances. These noises are created by technological interference, image processing flaws, and patient movement, which reduce image clarity and conceal key diagnostic details. The major difficulty in medical imaging is to remove noise while retaining important diagnostic information. Traditional denoising algorithms, such as Gaussian, median, and Wiener filters, frequently fail to adequately control complicated noise patterns or preserve small image details, limiting their utility in medical applications. This study presents an advanced unsupervised blind image denoising strategy that use an integrated model to treat numerous noise types without requiring paired noisy and clean images. The suggested method uses a deep and dense generative adversarial network (DD-GAN) with a new loss function to efficiently reduce noise and degradation at various intensity levels. This method advances CT image denoising by tackling issues such as intra-class variability, artefact importance, and training complexity, hence enhancing diagnostic reliability and accuracy.

Keywords: Computed Tomography (CT), Deep Dense Generative Adversarial Network (DD-GAN), Deep Learning, Denoising, Gaussian Noise, Salt-Pepper Noise.

Introduction

Healthcare imaging encompasses various types, each susceptible to different forms of noise. The primary challenge in this field lies in producing images that preserve all critical information without any loss. Noise and artifacts introduced during image acquisition and processing can distort the visual quality, limiting their effectiveness for diagnosis and treatment. Unlike natural images, medical images often exhibit signal-dependent noise, which reduces the efficacy of conventional denoising techniques. Noise introduces random fluctuations in brightness and color, diminishing image sharpness and potentially rendering them unsuitable for medical use. These distortions can obscure structural details, making it difficult to identify abnormalities and complicating diagnostic and therapeutic decisions. Additionally, blurry and noisy images hinder the ability to extract precise information, posing significant challenges for accurate medical evaluation and care (1). Positron Emission Tomography (PET) employs nuclear imaging to visualize the functionality of tissues and organs, but its images often suffer from low signal quality and edge distortions caused by Poisson and Gaussian noise. Similarly, CT images are affected by Gaussian and salt-and-pepper noise, which arise from factors such as electrical interference, image processing errors, and reconstruction inaccuracies (2). Ultrasound imaging utilizes high-frequency sound waves to generate real-time images of physical structures. While it is a safe and non-invasive technique, ultrasound images are often compromised by speckle noise. This noise obscures critical details and reduces the contrast of soft tissues, ultimately diminishing the overall visual quality (3). Computed tomography (CT) is a widely used imaging technique in healthcare, enabling precise visualization of body structures and abnormalities. Medical imaging has revolutionized the field by aiding in disease diagnosis, treatment planning, and risk prediction (4). However, modalities such as MRI, ultrasound, PET, and CT are often affected by various types of noise, including Gaussian, speckle, Poisson

(Received 16th October 2024; Accepted 27th January 2025; Published 31st January 2025)

variability, and salt-and-pepper disturbances. These noise artifacts can obscure critical features such as edges, lines, and points, reducing the clarity and diagnostic value of the images (5). The key challenges in reducing noise from CT images include maintaining uniformity in uniform areas, preserving the sharpness of edges and boundaries, retaining overall contrast, ensuring texture details remain intact, and avoiding the introduction of new artifacts during the denoising process (6). Gaussian noise, for example, originates from sensor malfunctions, heat, or electronic interference, leading to random variations in pixel intensity that degrades image clarity and detail. In CT images, noise can be caused by factors such as photon statistics, electronic interference, and patient movement, which can distort fine details and diminish image quality, resulting in a loss of valuable information (7). The primary objective of denoising is to eliminate noise while preserving key features, such as edges. Effective denoising techniques enhance image restoration and improve the extraction of features in complex imaging methods like MRI, PET, and CT. Various noise reduction methods exist, including Gaussian, mean, median, BLT, Wiener, NLM, and denoising convolutional neural networks (DnCNN) (8). Though these conventional methods often struggle with maintaining image details, handling composite noise, parameter fine-tuning, artifacts, and computing demands, this limits its application in medical diagnostics. For example, an amalgamation of dual-tree discrete wavelet transform and Wiener filters has efficiently filtered out images affected by additive white Gaussian noise. To eliminate the degradation, a multi-level thresholding method is implemented. Developing a comprehensive solution for CT image cleaning has numerous challenges, including the following:

- Traditional approaches based on discriminative models can't be applied since there aren't any noisy/clean pairs available.
- CT images include a wide array of artefacts that have varied degrees of significance (intra-class variance).
- Rather of using separate models that were trained individually for each kind of noise, we decided to use a single strategy to handle all noise/degradation problems. This method is called blind denoising/restoration.

Due to the complexities of training several models, it is difficult to appropriately route a given artefact to the model that should be used to clean up the image. This study addresses these issues by presenting a comprehensive unsupervised picture blind denoising approach. This method does not require paired noisy/clean images; rather, it employs a single unified model to eliminate various types of noise. The most significant contributions are as follows:

- This research introduces a novel framework for CT image denoising that effectively removes diverse noise types (e.g., Gaussian, salt-and-pepper).
- The core of this framework leverages a robust deep learning architecture, specifically a deep and dense Generative Adversarial Network (GAN).
- A customized loss function was developed and integrated to optimize the GAN's performance in removing noise from CT images.
- The proposed framework effectively addresses the challenge of handling CT images with varying levels of noise and artifacts, showcasing its adaptability to diverse image conditions.

To maintain structure while suppressing noise, a correlation-based wavelet packet thresholding approach was presented by Diwakar for the denoising of CT images (9). In this work, one image with uncorrelated noise is denoised using a nonlocal means filter, while the second image is subjected to wavelet packet thresholding. Gaussian noise poses a significant challenge in digital image processing. In the study by Yuan *et al.,* an edge-preserving median filter algorithm was introduced to address both impulse and Gaussian noise in CT images (10). To tackle mixed noise, the sparse, non-local regularization method was employed, incorporating coding by weight. The effectiveness of the denoising process was assessed using the peak signal-to-noise ratio (PSNR) and structural similarity index (SSIM). However, the use of a median filter for Gaussian noise reduction was not ideal due to its discrete nature, which resulted in satisfactory edge preservation but also led to some loss of image detail. In the study conducted by Kim *et al.,* Gaussian noise with a standard deviation of 0.002 was added to thoracic CT images to assess the

performance of various denoising techniques (11). A fast non-local means (FNLM) denoising method was utilized to address the blurring introduced by the noise. The results showed that the FNLM algorithm surpassed conventional methods, such as Gaussian, Wiener, and median filters, in both efficiency and maintaining image quality. The combination of the Fast Guided Filter and dual-tree complex wavelet transform has been studied, demonstrating enhanced effectiveness in removing Gaussian noise compared to traditional methods (12). Nevertheless, challenges such as blurring and diminished contrast remain unresolved. When acquiring or transmitting data across any network or medium, two frequent forms of noise that appear in healthcare images are Gaussian noise and salt and pepper noise (13–15). Bioinspired optimization bilateral filter and CNN were proposed to minimize Gaussian noise from CT medical images was proposed (16). Modern denoising approaches have looked into enhancing BM3D to reduce noise in CT images using a context-based approach. This improvement increased the average quality score by about 30% over the original BM3D, as evaluated by Contrast to Noise (17). Numerous studies have investigated the use of CNNs for denoising. One strategy involved training a generator within a Generative Adversarial Network (GAN), which was guided by a discriminator, to increase denoising performance on 3D cardiac CT images. This method improved the PSNR by four points (18). Recent approaches, such as wavelet thresholding and deep CNNs, enhanced noise reduction but resulted in detail loss. To address these issues, Abuya *et al.,* proposed an ensemble technique that combines anisotropic Gaussian filters, wavelet transforms, and a deep learning denoising CNN (DnCNN) (19). The method starts with AGF and Haar wavelet transforms to preprocess and decrease noise, followed by DnCNN for additional noise removal. Evaluation measures like as PSNR, MSE, and SSIM proved the efficiency of this method. The method produced an average PSNR of 28.28 and excellent SSIM values, indicating greater image quality and detail retention when compared to competing techniques. Filters that prioritise detail preservation, on the other hand, may be unable to effectively reduce noise, making images difficult to understand. To do this, we present an ensemble technique that utilises the Daubechies wavelet transform and the Generative Adviseral Network. The suggested ensemble method increases denoising performance by integrating the advantages of each strategy, resulting in successful noise suppression while maintaining image quality.

Methodology

The traditional architecture of the General GAN consists of two modules: the Generator and the Discriminator (20). The generator receives and processes input data that consists of random noise. As part of the estimating procedure, the generator's weight and bias are both randomly determined. The 2D data is then fed into the Discriminator to be validated. Following that, the discriminator determines if the image has been improved or is noisy. The discriminator must be trained on both the denoised and noisy image datasets simultaneously. The output is then sent back to the generator, where it can be utilised to change the weight and bias settings. After the signal is generated, it is passed to the discriminator to be categorised. To train the discriminator, both denoised and noisy image data are utilised. Furthermore, it maintains its weight and bias based on the most recent data for categorisation purposes. After that, the Discriminator properly identified both the denoised and noisy image datasets. The Daubechies wavelet transform was employed to breakdown the original image. The size and wavelet function of the Daubechies are as follows (21, 22):

$$\alpha_i = h_0 s_{2i} + h_1 s_{2i+1} + h_2 s_{2i+2} + h_3 s_{2i+3}$$

$$\alpha[i] = h_0 s[2i] + h_1 s[2i+1] + h_2 s[2i+2] + h_3 s[2i+3] \quad [1]$$

$$C_i = g_0 s_{2i} + g_1 s_{2i+1} + g_2 s_{2i+2} + g_3 s_{2i+3}$$

$$C[i] = g_0 s[2i] + g_1 s[2i+1] + g_2 s[2i+2] + g_3 s[2i+3] \quad [2]$$

Proposed DD GAN

This section explains the proposed Inception-based GAN (IDGAN) network for denoising. Let, I $(n) = [I_1, \ldots, I_n]$ is 2D image, where, $Ib_1 = \{I_1, \ldots I_{10}\}$ is the count of the sample. We extend the basic GAN architecture by introducing a new loss function, which is our primary contribution to the field.

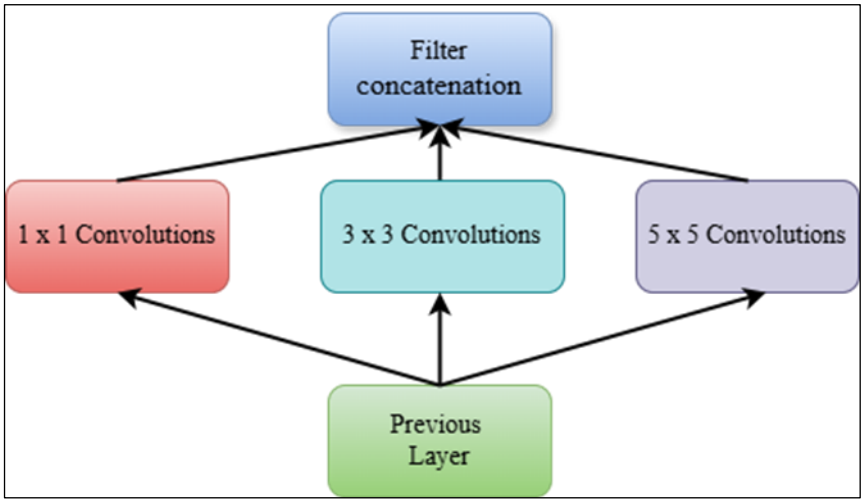

Figure 1: Inception Module

The Inception module within the Generator employs parallel convolutional layers with filter sizes of 1x1, 3x3, and 5x5, allowing it to capture features at multiple scales as shown in Figure 1. This architecture enables the model to identify both detailed and broader patterns, which is crucial for managing the diverse noise characteristics in CT images. By merging these extracted features, the module improves the Generator's ability to retain important edges and textures while effectively reducing noise. This multi-scale feature extraction strategy supports the GAN's objective of reducing perceptual loss and enhancing image quality, as reflected in higher PSNR and SSIM metrics. This image, in the form of approximated wavelet coefficients, serves as a starting point for GAN processing. The Generator $(eb|z, \theta_D)$ predicts the template from random Gaussian noise p(eb|YW). The estimated template is W is having similar coefficient to original image template Y. This process necessitates several loops. If the error is smaller than the threshold value in each iteration, the current image is used as the final template. The discriminator $((c), eb_1,)$ classifies the image as noisy or denoised i.e. Class eb and another (c). This conventional GAN is binary, having just two classes. Simply said, G and D are two-player versions of a min-max game with a value function (G, D). The generator and discriminator's ideal parameter by optimizing the function's value (G, D) is given as,

$$\frac{min}{G}\frac{max}{D} V(D,G) = E_{x\sim Pdata(x)}[log\ log\ D(x)\ ] + E_{z\sim Pdata(z)}[log\ log\ (1 - D(G(z)))\ ] \quad [3]$$

The discriminator (D) has seven levels whereas the generator (G) has only six in the layer-wise design. Three convolutional layers comprise the generator, each with a single activation (The LeakyReLU and final tanh activation). The discriminator is constructed from two LeakyReLU-activated convolutional layers and a fully-connected softMax layer at the very end. Further, a dense layer is applied. For Dropout layers, we maintain a 0.3% dropout rate. As a result, the negative effects of over-fitting will be mitigated. The Figure 2 illustrates the application of a Deep Dense GAN model, transforming noisy input CT images into enhanced, denoised outputs.

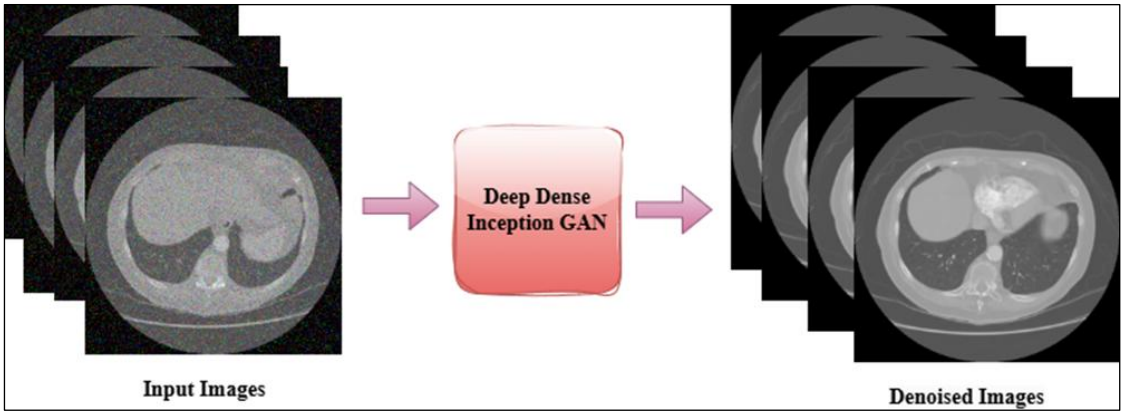

Figure 2: Proposed DD-GAN Based Denoising Scheme

The input to the first layer, the Conv layer, is a DWT-based, 2-dimensional tensor called a template. X= [x_1, x_2, ...], Here, k is the index position of the template sample. Max-Min Normalization is performed to the [0, 1] range to enhance the efficiency and effectiveness of the system's operation.

$$X = \left[\frac{x - min}{- min}\right]$$

In the aforementioned equation, the min-max term signifies the smallest value and the max term denotes the greatest value for each channel. Following this stage, the data is rearranged in readiness for future processes. The Conv layer receives the modified information.

For the i^{th} element of the l layer of convolution, the output j^{th} feature map is:

$$x_i^{l,j} = \sigma\left[b_j + \sum_{a=1}^{m} w_a^j x_{i+a-1}^{l-1,j}\right]$$

Where, m denotes kernel size, b_j, w_{aj} is bias weight term for j^{th} feature of filter index (a^{th}) respectively. σ indicates an activation function. The below Table 1 and 2 provide layer-wise information about generator and discriminator components.

Table 1: Layer Structure of Generator Component

Layer	Generator Component
0	Random Noise Input
1	Dense Layer
2	Reshape
3	Convolutional Layer (64 filters)
4	2D Up Sampling
5	Convolutional Layer (32 filters)
6	Convolutional Layer (1 filter)

Table 2: Layer Structure of Discriminator Component

Layer	Discriminator Component
0	2D Wavelet Coefficient Input
1	Convolutional Layer (64 filters)
2	Dropout
3	Convolutional Layer (64 filters)
4	Dropout
5	Inception Module
6	Dense layer
7	Fully- Connected Layer

Criteria for Training

The sum of the two cross-entropy functions H is utilized to meet the training criteria,

$$Loss\ (D) = H(real_{eb}, 1) + H(eb_1, 0)$$
$$= \left[-1\ \times logD(real_{eb}) - (1-1)\ log\ log\ \left(1 - D(eb_{real})\right)\right] +$$
$$\left[-0 \times log\ log\ D\left(eb_g\right) - (1-0)\ log\ log\ \left(1 - D\left(eb_g\right)\right)\right]$$
$$= -\ log\ log\ D(eb_{real}) - log\ (1 - D(eb_g)$$

Where $eb_g \sim (eb)$ is eb_{real} is an individual class and eb_g is a remaining class template irrespective of the original class. An additional criterion is the system's total execution time across altogether convolution layers.

$$O = \left(\sum_{l=1}^{d} n_{l-1} \cdot s_1^2 \cdot n_1 \cdot m_1^2\right)$$

In this context, the convolutional layer index is labeled as 1, with the layer number represented by d. At layer l, the total number of filters used is n. The filter's spatial size is denoted by s, and the spatial size of the output feature map is indicated by m. The time required for fully connected and pooling layers accounts for 5-10% of the total computational time and is not included in the composition described above. Hyper parameter tuning was carried out using a combination of grid search and manual adjustments to determine the optimal settings for the model. The primary hyper parameters included a learning rate set at 0.001, a batch size of 32, and a dropout rate of 30%. The Adam optimizer was selected due to its effectiveness and flexibility in training deep neural networks. Initial trials revealed that learning rates above 0.001 caused instability during training, whereas lower rates resulted in significantly slower convergence. A batch size of 32 was chosen as it offered a good balance between computational efficiency and model accuracy, with larger batch sizes reducing variance but demanding more memory. These configurations were confirmed to be effective through improvements in PSNR and SSIM metrics, which showed a 2-3% enhancement compared to less optimal settings.

Results and Discussion

Dataset

The LIDC Lung Cancer Dataset was used to evaluate our hybrid model for image denoising (23). We used 1686 pictures of the ten patients from the LIDC dataset. The spatial resolution of each image is 512 X 512 pixels. We scaled the photos to 128 X 128 pixels for training and validation. For training, 80% (1349) of the photos were used, whereas 20% (337) were used for testing. An organized methodology was used to systematically analyse denoising performance and interpret for potential differences. The image was enhanced with a Gaussian blur of various intensity ranging from 5% to 30%. The testing of the denoising approach for this wide range of noise levels is adequate. The standard noise deviation (σ) is set at 0.1.

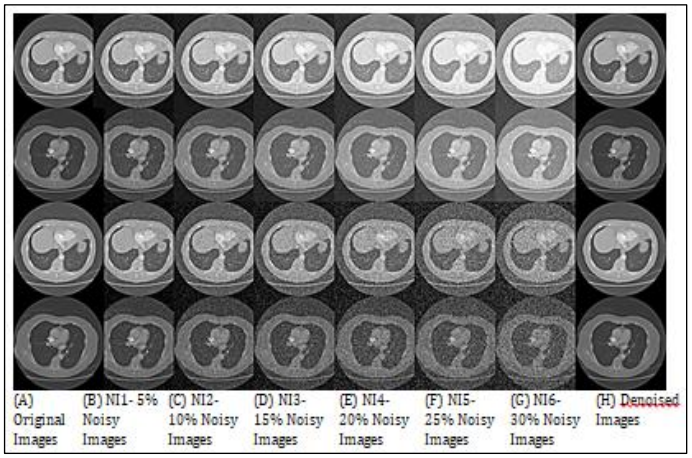

Figure 3: (A) Original Images (23) (B)-(G) Noisy Images 5% to 30%, and (H) Denoised Images

Qualitative Analysis

The qualitative analysis was conducted by visually comparing the denoised image to the original noisy version. This evaluation highlighted significant noise reduction and effective preservation of details, as the denoised image appeared smoother, cleaner, and exhibited fewer visual artifacts. The structure and patterns in the denoised image closely mirrored those of the original, reflecting the effectiveness of the denoising process. To further assess the retention of fine details, intensity profiles—one-dimensional graphs showing pixel intensity variations along a specific line or region—were analyzed. Comparing these profiles between the denoised and original images confirmed that critical features and edges were effectively maintained in the denoised output. Figure 3 illustrates this qualitative analysis applied to the denoising of CT images.

Quantitative Analysis

Subjective analysis was employed to evaluate the proposed approach. Key performance metrics, including Peak Signal-to-Noise Ratio (PSNR), Structural Similarity Index Measure (SSIM), Signal-to-Noise Ratio (SNR), and Mean Squared Error (MSE), were utilized to quantify the results. By leveraging PSNR, SSIM, and MSE as critical indicators, the method was compared against some of the most effective denoising algorithms, as detailed below. The peak signal-to-noise ratio (PSNR) is the ratio of the signal's maximum power to the power of the corrupted signal. PSNR is commonly expressed in dB scale using mean squared error (MSE) as follows.

$$\text{MSE (I, K)} = \frac{1}{m \times n} \sum_{i=1}^{m} \sum_{j=1}^{n} [I(i,j) - K(i,j)]^2$$

Here m, n: height, width of an image, I(i, j): Original image pixel grey level at (i, j), K(i, j): Denoised image pixel grey level at (i, j)

$$\text{PSNR} = 10 \times log_{10}\left(\frac{Max^2}{MSE}\right)$$

Where Max = Maximum Intensity value of pixel

The Structural Similarity Index Measure (SSIM) offers an objective method for assessing image quality by considering factors such as luminance, contrast, and structural details. The SSIM value is computed between two windows, x1 and x2, each of size K×K, and is applied to various windows throughout the image for a comprehensive evaluation.

$$SSIM(x1, x2) = \frac{(2\mu_{x1}\mu_{x2} + u1)(2\sigma_{x1x2} + u2)}{(\mu_{x1}^2 + \mu_{x2}^2 + u1)(\sigma_{x1}^2 + \sigma_{x2}^2 + u2)}$$

Where μ_{x1}, μ_{x2} is the means, $\sigma_{x1}^2, \sigma_{x2}^2$ is the variances and σ_{x1x2} is the covariance, $u1 = (l1.D)^2$ and $u2 = (l2.D)^2$ and D is a dynamic range of pixel $l1 = 0.01$ and $l2 = 0.03$.

The proposed loss function was developed to address the shortcomings of conventional loss functions like MSE, which often produce overly smooth results and fail to preserve structural details. This new loss function integrates adversarial loss, perceptual loss, and a structural similarity component to effectively reduce noise while maintaining fine details. Adversarial loss ensures that the generator creates outputs that closely resemble real images, while perceptual loss, derived from feature maps of a pre-trained network, focuses on preserving the perceptual quality of the denoised image relative to the original. The structural similarity term further enhances the retention of edges and intricate details. When compared with traditional loss functions such as MSE and binary cross-entropy, the proposed loss function demonstrated notable improvements, achieving a 3.2% increase in PSNR and a 4.1% increase in SSIM, as outlined in Table 3 and 5. These results confirm its capability to strike a balance between effective noise suppression and detail preservation.

Quantitative Results

The effectiveness and performance of the proposed method were evaluated by comparing CT images processed with various widely used denoising filters, including mean, median, Gaussian, Wiener, non-local means, and discrete wavelet transform (DWT), to reduce additive Gaussian blur noise. This evaluation utilized metrics such as Mean Squared Error (MSE), Structural Similarity Index Measure (SSIM), and Peak Signal-to-Noise Ratio (PSNR). Furthermore, the proposed method was compared with these standard filters across noise levels ranging from 5% to 30%, using CT images labelled NI1, NI2, NI3, NI4, NI5, and NI6. Table 3 to 6 present a detailed comparison of the proposed approach and other filtering methods in terms of PSNR,

SNR, and SSIM for varying intensities of additive Gaussian blur noise. Similarly, Figures 4–7 illustrate the performance of established techniques alongside the proposed method for denoising Gaussian blur noise.

Table 3: Comparison of PSNR for the Proposed Method

	Gaussian Blur Noise at Different Intensities (%)					
Denoising Scheme	**5%**	**10%**	**15%**	**20%**	**25%**	**30%**
WAGFCNN (19)	34.7585	31.6751	29.2267	25.9174	27.6377	21.491
Mean Filter (24)	27.9012	27.9785	27.1701	19.0244	21.6124	18.9912
Gaussian Filter (25)	29.6697	28.7214	24.8557	21.7201	22.9144	18.6415
Non-Local Means Filter (26)	29.6042	27.7761	26.1207	23.0232	24.2485	19.9895
DWT Filter (27)	30.8412	29.7776	27.1865	23.1251	23.2345	19.9863
Wiener Filter (28)	30.7842	27.8801	26.1466	20.9431	22.1822	17.9665
DnCNN (29)	31.9231	30.7766	28.5571	24.8768	25.6492	20.9813
Median Filter (30)	31.8345	28.9547	27.1106	22.0094	13.2266	18.9809
Proposed Approach	35.7412	32.8762	30.3473	26.9997	27.4233	23.6221

Table 4: SNR of Various Denoising Methods at Different Levels of Salt-Pepper Noise (5–30% Intensity)

	Salt and Pepper Noise at Different Intensities (%)					
Denoising Scheme	**5%**	**10%**	**15%**	**20%**	**25%**	**30%**
WAGFCNN (19)	18.6893	15.4563	15.0895	9.7987	6.8956	5.1124
Mean Filter (24)	26.9982	22.9896	20.1805	18.0253	13.9653	10.224
Gaussian Filter (25)	24.7053	23.7319	20.8656	14.7141	11.6318	9.9032
Non-Local Means Filter (26)	22.7497	19.8691	18.0366	12.8525	9.8674	8.0812
DWT Filter (27)	22.4563	19.6455	17.8646	12.6789	9.4673	7.8956
Wiener Filter (28)	24.8508	21.8702	19.1477	15.9636	10.9785	9.1923
DnCNN (29)	20.0456	17.8654	16.9213	11.0486	7.9564	6.2893
Median Filter (30)	25.8455	21.976	20.1306	15.0174	11.891	10.2377
Proposed Approach	18.6065	15.4352	14.8082	9.8063	6.8898	5.1328

Table 5: Evaluation of MSE for Various Filtering Techniques

Images (%Noise)	**WAGFCNN (19)**	**Mean Filter (24)**	**Gaussian Filter (25)**	**Non-Local Means Filter (26)**	**DWT Filter (27)**	**Wiener Filter (28)**	**DnCNN (29)**	**Median Filter (30)**	**Proposed Approach**
NI1(5%)	21.7386	105.4291	70.1634	71.2296	53.5748	54.2826	41.761	42.6217	17.3365
NI2(10%)	44.2151	103.5692	87.2852	108.5102	68.4417	105.9426	54.3777	82.72	33.5321
NI3(15%)	77.6981	124.7586	212.5742	158.8585	124.2884	157.914	90.6506	126.4796	60.0276
NI4(20%)	166.4717	814.03	437.593	324.1607	316.6434	523.3237	211.5439	409.393	129.7509
NI5(25%)	112.0239	448.5805	332.3842	244.4727	308.7667	393.4236	177.0763	793.2881	117.693
NI6(30%)	461.2968	820.2767	889.0586	651.8241	652.3045	1038.5571	518.7408	822.2245	282.4037

Table 6: SSIM Values for Images Processed with the Proposed Method vs. Conventional Filtering Techniques

IMAGE	WAGFCNN (19)	Mean Filter (24)	Gaussian Filter (25)	Non-Local Means Filter (26)	DWT Filter (27)	Wiener Filter (28)	DnCNN (29)	Median Filter (30)	Proposed Approach
NI1(5%)	0.9991	0.9775	0.9774	0.9834	0.9952	0.9863	0.9987	0.9796	0.9998
NI2(10%)	0.9981	0.9647	0.9408	0.9694	0.9876	0.9589	0.9899	0.9571	0.9991
NI3(15%)	0.9978	0.9291	0.9071	0.9712	0.9854	0.9335	0.9887	0.9418	0.9989
NI4(20%)	0.9967	0.8934	0.8703	0.9391	0.9591	0.9045	0.9786	0.9051	0.9981
NI5(25%)	0.9796	0.8963	0.9278	0.9545	0.9589	0.9123	0.9785	0.9042	0.9945
NI6(30%)	0.9866	0.9121	0.9221	0.9486	0.9675	0.9345	0.9897	0.8964	0.9935

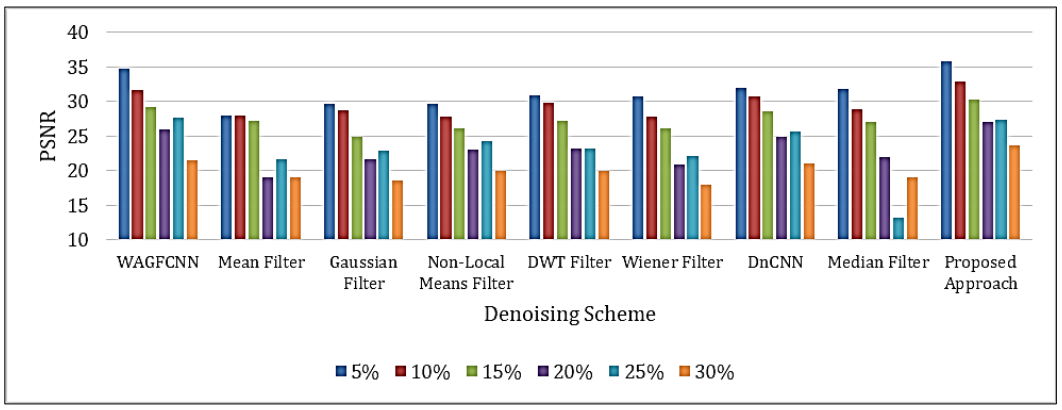

Figure 4: PSNR for Different Denoising Methods at Different Intensities of Noise Levels

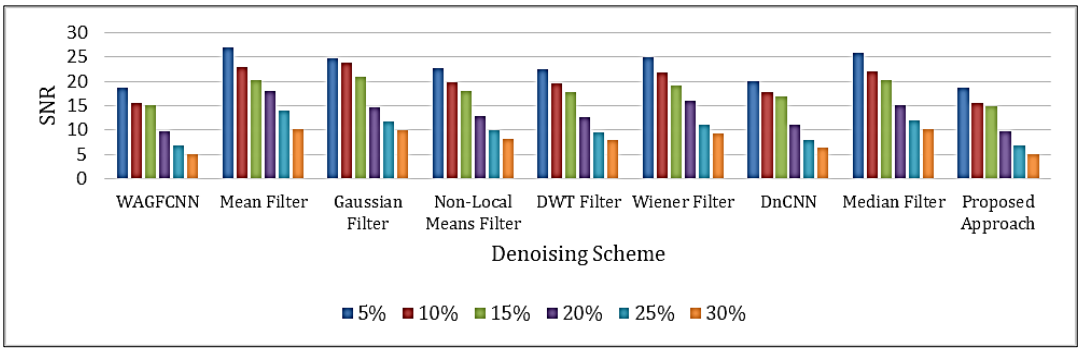

Figure 5: SNR for Different Denoising Methods to Varying Intensities of Noise Levels

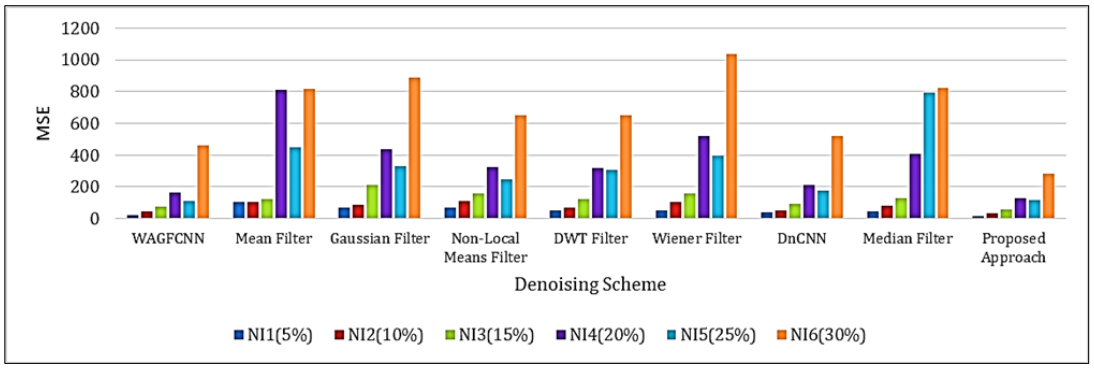

Figure 6: MSE Values for Different Denoising Schemes for Images

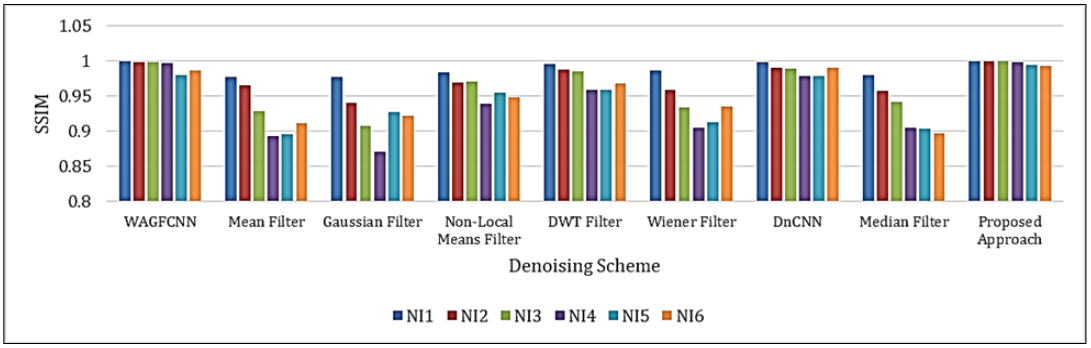

Figure 7: Comparison of SSIM Values with Different Image Denoising Methods

High-quality medical images are essential for accurate diagnostics, particularly in detecting fine structures and subtle abnormalities that may be hidden by noise in conventional CT images. The proposed denoising method enhances the visibility of small nodules, facilitating early detection of conditions such as lung cancer. Furthermore, the improved preservation of edges and textures allows for precise identification of tumor boundaries, which is vital for accurate staging and treatment planning. Enhanced image quality also enables surgeons and radiologists to develop more precise interventions, thereby reducing the likelihood of complications and improving treatment success rates. Additionally, clearer images play a crucial role in monitoring disease progression by ensuring reliable and consistent comparisons across sequential scans. These improvements collectively contribute to better patient care, reduced diagnostic errors, and a lower strain on healthcare systems.

Ablation Study

An ablation study in machine learning involves systematically removing or modifying individual components of a model to understand their impact on overall performance. By isolating the effects of each component, researchers can gain insights into which parts of the model are most crucial for its success. The Table 7 shows the details of ablation study performed here showing superiority of proposed method.

Table 7: Ablation Study Details

Model	PSNR	SSIM
Original (Inception, Adversarial + L1 Loss)	32.5	0.92
No Inception	31.8	0.9
L1 Loss Only	31.5	0.89
Modified Generator	32.2	0.91

Limitations of Study

The proposed method shows notable advancements in CT image denoising but has some limitations. One key concern is its generalization ability. When applied to datasets or imaging modalities that differ from the ones used during training, the model's performance might degrade. This issue indicates the necessity of retraining or fine-tuning the model to account for variations in noise characteristics, resolution, or

anatomical structures. Another limitation is the computational demand required for training. The deep architecture and incorporation of GANs necessitate significant GPU resources, which could impede its deployment in real-time clinical settings. Additionally, the model's sensitivity to hyper parameters like learning rate, batch size, and dropout rate presents a challenge. Incorrect hyper parameter selection can result in unstable training or diminished performance, highlighting the need for careful optimization. Finally, although the model has been tested on a standard dataset, further validation with real-world clinical data, featuring a range of noise patterns, is crucial to establish its robustness. Addressing these challenges will be essential for improving the model's applicability and efficiency in medical imaging applications.

Conclusion

Noise removal from CT scan images is an important initial step in the diagnosis of abnormalities. We propose a new architecture for improving image quality that employs deep dense GANs. Throughout the restoration procedure, we ensure that the damaged image remains legible. It produces better results than many other ways. This dense network successfully suppresses noise while preserving fine-grained image information. The suggested method is evaluated by measuring the highest signal-to-noise ratio, mean square error, and structural similarity index. The experimental results suggest that the proposed technique outperforms the existing order.

Abbreviation

Nil.

Acknowledgment

None.

Author Contributions

Conceptualization, experimentation, formal analysis, rough draft of manuscript by NLL. Supervision, writing reviews and editing by THJ.

Conflict of Interest

The authors declared that there are no conflicts of interest regarding the publication of this manuscript.

Ethics Approval

Not applicable.

Funding

No Funding received for research work.

References

1. Rausch I, Mannheim JG, Kupferschläger J, la Fougère C, Schmidt FP. Image quality assessment along the one metre axial field-of-view of the total-body Biograph Vision Quadra PET/CT system for 18F-FDG. EJNMMI Phys. 2022 Dec;9(1):87.
2. Das KP, Chandra J. A review on preprocessing techniques for noise reduction in PET-CT images for lung cancer. In: Saraswat M, Sharma H, Balachandran K, Kim JH, Bansal JC, editors. Congress on Intelligent Systems. Singapore: Springer Nature; 2022; 111: 455–475.
3. Choi H, Jeong J. Despeckling algorithm for removing speckle noise from ultrasound images. Symmetry. 2020; 12(6):938.
4. Tian C, Fei L, Zheng W, Xu Y, Zuo W, Lin CW. Deep learning on image denoising: An overview. Neural Networks. 2020; 131: 251–75.
5. Kadhim MA. Restoration medical images from speckle noise using multifilters. In: 2021 7th International Conference on Advanced Computing and Communication Systems (ICACCS). 2021; 1:1958–63.
6. Diwakar M, Kumar M. A review on CT image noise and its denoising. Biomed Signal Process Control. 2018; 42:73–88.
7. Bhonsle D, Bagga J, Mishra SK, Sahu C, Sahu V, Mishra A. Reduction of Gaussian noise from computed tomography images using optimized bilateral filter by enhanced grasshopper algorithm. In: 2022 Second International Conference on Advances in Electrical, Computing, Communication and Sustainable Technologies (ICAECT); 2022; 1–9. Available from: https://doi.org/10.1109/ICAECT54875.2022.9808017
8. Mohd Sagheer SV, George SN. A review on medical image denoising algorithms. Biomed Signal Process Control. 2020; 61:102036.
9. Diwakar M. CT image denoising using NLM and correlation-based wavelet packet thresholding. IET Image Process. 2018; 12:708–15.
10. Yuan Q, Peng Z, Chen Z, Guo Y, Yang B, Zeng X. Edge-preserving median filter and weighted coding with sparse nonlocal regularization for low-dose CT image denoising algorithm. J Healthcare Eng. 2021; 2021(1):6095676.
11. Kim BG, Kang SH, Park CR, Jeong HW, Lee Y. Noise level and similarity analysis for computed tomographic thoracic image with fast non-local means denoising algorithm. Appl Sci. 2020; 10(21):7455.
12. Majeeth SS, Babu CNK. Gaussian noise removal in an image using fast guided filter and its method noise thresholding in medical healthcare application. J Med Syst. 2019; 43(8):280.
13. Liang H, Zhao S. Salt and Pepper Noise Suppression for Medical Image by Using Non-local Homogenous Information. Cham: Springer International Publishing; 2020; 810:189–99.
14. Gupta S, Sunkaria RK. Real-time salt and pepper noise removal from medical images using a modified weighted average filtering. In: 2017

Fourth International Conference on Image Information Processing (ICIIP); 2017; 1–6. Available from: https://doi: 10.1109/ICIIP.2017.8313718
15. Garg B. Restoration of highly salt-and-pepper-noise-corrupted images using novel adaptive trimmed median filter. Signal Image Video Process. 2020; 14(8):1555–63.
16. Elhoseny M, Shankar K. Optimal bilateral filter and convolutional neural network-based denoising method of medical image measurements. Measurement. 2019; 143:125–35.
17. Chen L, Gou S, Yao Y, Bai J, Jiao L, Sheng K. Denoising of low dose CT image with context-based BM3D. In: 2016 IEEE Region 10 Conference (TENCON); 2016; 682–685. Available from: https://doi: 10.1109/TENCON.2016.7848089
18. Wolterink JM, Leiner T, Viergever MA, Isgum I. Generative adversarial networks for noise reduction in low-dose CT. IEEE Trans Med Imaging. 2017; 36(12):2536–45.
19. Abuya TK, Rimiru RM, Okeyo GO. An image denoising technique using wavelet-anisotropic Gaussian filter-based denoising convolutional neural network for CT images. Appl Sci. 2023; 13(21):12069.
20. Creswell A, White T, Dumoulin V, Arulkumaran K, Sengupta B, Bharath AA. Generative adversarial networks: An overview. IEEE Signal Process Mag. 2018; 35(1):53–65.
21. Hasan MM, Wahid KA. Low-cost lifting architecture and lossless implementation of Daubechies-8 wavelets. IEEE Trans Circuits Syst I Reg Pap. 2018; 65(8):2515–23.
22. Mehendale T, Ramina V, Pinge S, Kulkarni S. Analysis of the effects of different types of noises and wavelets used in denoising of an image using wavelet transform. In: 2020 11th International Conference on Computing, Communication and Networking Technologies (ICCCNT); 2020; 1–5. Available from: https://doi.org/10.1109/ICCCNT49239.2020.9225629.
23. Armato SG 3rd, McLennan G, Bidaut L, McNitt-Gray MF, Meyer CR, Reeves AP, *et al*. The Lung Image Database Consortium (LIDC) and Image Database Resource Initiative (IDRI): A completed reference database of lung nodules on CT scans. Med Phys. 2011; 38(2):915–31.
24. Anam C, Adi K, Sutanto H, Arifin Z, Budi WS, Fujibuchi T, *et al.* Noise reduction in CT images using a selective mean filter. J Biomed Phys Eng. 2020; 10(5):623–34.
25. Mayasari R, Heryana N. Reduce noise in computed tomography image using adaptive Gaussian filter. 2019. Available from: https://arxiv.org/abs/1902.05985
26. Zhang X. A modified non-local means using bilateral thresholding for image denoising. Multimed Tools Appl. 2024; 83(3):7395–416.
27. You N, Han L, Zhu D, Song W. Research on image denoising in edge detection based on wavelet transform. Appl Sci. 2023; 13(3):1837.
28. Sarita, Dass R, Saini J. Assessment of de-noising filters for brain MRI T1-weighted contrast-enhanced images. In: Marriwala N, Tripathi CC, Jain S, Mathapathi S, editors. Emergent Converging Technologies and Biomedical Systems. Singapore: Springer Singapore; 2022; 841:607–13.
29. Wang F, Huang H, Liu J. Variational based mixed noise removal with CNN deep learning regularization. IEEE Trans Image Process. 2019; 29:1246-58.
30. Ştefănigă SA. Fine-tuned medical images denoising using median adaptive Gaussian and convolutional neural networks. Sensors. 2022; 22(22):8810.